2017

3D Modeling and Characterization of a Calorimetric Flow Rate Sensor for Sweat Rate Sensing Applications

A. T. Iftekhar
J. C.T. Ho
A. Mellinger
Dr. Tolga Kaya, *Sacred Heart University*

.

3D modeling and characterization of a calorimetric flow rate sensor for sweat rate sensing applications

Ahmed Tashfin Iftekhar, Jenny Che-Ting Ho, Axel Mellinger, and Tolga Kaya

Citation: Journal of Applied Physics **121**, 094505 (2017); doi: 10.1063/1.4977998
View online: http://dx.doi.org/10.1063/1.4977998
View Table of Contents: http://aip.scitation.org/toc/jap/121/9
Published by the American Institute of Physics

JOURNAL OF APPLIED PHYSICS **121**, 094505 (2017)

3D modeling and characterization of a calorimetric flow rate sensor for sweat rate sensing applications

Ahmed Tashfin Iftekhar,[1] Jenny Che-Ting Ho,[1] Axel Mellinger,[2,3] and Tolga Kaya[1,3,a)]
[1]*School of Engineering and Technology, Central Michigan University, Mt. Pleasant, Michigan 48859, USA*
[2]*Department of Physics, Central Michigan University, Mt. Pleasant, Michigan 48859, USA*
[3]*Science of Advanced Materials Program, Central Michigan University, Mt. Pleasant, Michigan 48859, USA*

(Received 12 December 2016; accepted 22 February 2017; published online 7 March 2017)

Sweat-based physiological monitoring has been intensively explored in the last decade with the hopes of developing real-time hydration monitoring devices. Although the content of sweat (electrolytes, lactate, urea, etc.) provides significant information about the physiology, it is also very important to know the rate of sweat at the time of sweat content measurements because the sweat rate is known to alter the concentrations of sweat compounds. We developed a calorimetric based flow rate sensor using PolydimethylSiloxane that is suitable for sweat rate applications. Our simple approach on using temperature-based flow rate detection can easily be adapted to multiple sweat collection and analysis devices. Moreover, we have developed a 3D finite element analysis model of the device using COMSOL Multiphysics™ and verified the flow rate measurements. The experiment investigated flow rate values from 0.3 μl/min up to 2.1 ml/min, which covers the human sweat rate range (0.5 μl/min–10 μl/min). The 3D model simulations and analytical model calculations covered an even wider range in order to understand the main physical mechanisms of the device. With a verified 3D model, different environmental heat conditions could be further studied to shed light on the physiology of the sweat rate. *Published by AIP Publishing.*
[http://dx.doi.org/10.1063/1.4977998]

I. INTRODUCTION

Athletes and military personnel constantly push themselves physically and emotionally during training as well as in combat or a competition. Physical exertion often results in improper levels of body fluids. One of the main mechanisms of body temperature regulation occurs through sweat. Sweating is a physiological process to regulate core body temperature. It is known that losses of more than 2% of body weight (BW) during an activity causes degradation in physiological functions.[1–5] More than 3% loss of BW in a physically demanding task increases the risk of heat cramps, even heat stroke.[1] Sweat contains mainly water and electrolytes such as sodium, potassium, magnesium, calcium, urea, lactate, and minerals.[6,7] It has been reported that the concentration of sweat compound differs greatly with gender, fitness level, location of the sweat sampling site on the human body, and environmental conditions.[6,8–12] Although knowing the constituents of sweat provides significant information, the rate of sweat is also crucial as it alters the sweat concentration significantly.[13]

The human body has two types of sweat glands; eccrine (responsible mainly for thermoregulation) and apocrine (sweat produced mostly due to excitement). Eccrine sweat glands are distributed around the body surface whereas apocrine sweat glands are located mostly on groin areas and under armpits.[7] The distribution of eccrine sweat glands over the body is not uniform. It is reported that volar surfaces of the hand and foot have 500 glands/cm^2, and the dorsal forearm skin has around 135–145 glands/cm^2.[6] An eccrine sweat gland has a secretory and ductal region.[6,7,14] Sweat produced in the secretory coil (isotonic and similar to the interstitial fluid) travels to the distal duct where the electrolytes in sweat are mostly reabsorbed and sweat becomes hypotonic.[6,7,14] However, it is known that electrolyte reabsorption depends on the sweat rate and also on the capacity for the channel to reabsorb electrolytes.[15,16] Increased sweat rate decreases the electrolyte reabsorption in the ductal region, which would eventually lead to an increased electrolyte loss through sweating.[13,17–19]

Although the sweat electrolyte concentration is considered to be a good indicator for hydration status, it is known that the sweat rate also impacts the sweat concentration.[13,20] Getting sweat rate data would indeed provide us with additional information and help an athlete or soldier decide how much water and electrolytes he/she should intake during a physically demanding activity in order to keep him/her at peak performance physically and mentally.[13] The whole body sweat rate can be measured by using a Whole Body Wash-Down (WBW) technique, where sweat is collected during exercise, following the wash-down of the equipment and subject with water containing ammonium sulfate which is not present in sweat.[21] The sweat rate can also be obtained from the body mass difference between before and after exercise. Absorbent pads have also been utilized to collect sweat from shoulders, chest, or thighs in order to determine local sweat rates.[22–26] However, both WBW and absorbent pad techniques cannot provide real-time sweat rate data. A ventilated capsule approach has emerged to measure the sweat rate in real-time with relatively bulky measurement setups that make them non-portable.[11,27–29] Primarily used for infants,

[a)]Author to whom correspondence should be addressed. Electronic mail: kaya2t@cmich.edu

Macroduct sweat collectors can be useful for measuring both the sweat rate and sweat data with additional equipment.[30]

Recently, engineers have begun to develop real-time sweat rate sensors based on micromachined hygrometers and capacitive sweat absorbers. A device was developed adding a sweat absorber, a flexible substrate (kapton tape) with interdigitated electrodes, and a communication hub for the real time sweat rate sensor.[31] As the absorber collects the sweat, capacitance of the sensor changes to monitor the sweat rate for a limited time (due to limited absorbance on the absorbent).[31] A textile based wearable sweat-rate sensor was developed based on Fick's diffusion law in which the vapor pressure gradient was measured from two humidity sensors at different heights from the skin to calculate the sweat rate.[32] Another capacitive humidity sensor with a vapometer as a reference was used to determine the rate of sweat.[32,33] Image analysis for the detection of the sweat rate has also been reported by utilizing Macroduct.[34]

It is widely accepted that microflow sensing (flow rates around μl/min) can be implemented with thermal flow rate sensors, particularly calorimetric or thermal pulse flow sensors.[35–38] A thermal anemometer flow sensor was conceptualized and validated with simulations.[38] The theory of the thermal flow sensors and effects of geometry were also reviewed.[35,36] A few studies used COMSOL Multiphysics for 2D computational modeling of calorimetric flow rate meters.[37,39] Furthermore, Sabate *et al*. built a micromachined flow sensor and conducted some preliminary numerical simulations.[42] Their 2D simulations provided very useful insights but needed improvement by considering 3D effects and boundary conditions. Additionally, the heater temperature selected for their simulations was 150 °C, which is considered quite high for human applications. Lastly, Sabate's experiments were performed using Nitrogen gas.[42]

For liquid micro flow rate sensors, only a limited amount of research has been carried out. In Lammerink's study, the flow channel for measuring micro-liquid flow was 1 mm × 0.5 mm and they used temperature sensors symmetrically distanced from the heater.[43] A supporting beam was used for the heater and the sensors in the x–y plane, and the geometry was designed in a way that the heat transport in the side walls was less than the heat transport in the ceiling and the floor of the model. Different types of media (water, 2-propanol, and air) were used in the experiment, and the sensitivity of the device was found to be dependent on the thermal diffusivity of the medium.[43] Two additional resistors were used to avoid parasitic series resistances. This work did not elaborate on boundary conditions of the numerical model and not discuss the heater power and cooling effects of the flow. Nguyen and Dötzel introduced the concept of heater and temperature sensor arrays positioned asymmetrically in a 1.33 mm × 0.5 mm channel. As they mentioned, the assumptions in approximating the thickness of the thermal boundary layer in their analytical model were not suitable for microflow sensing; hence, their model only provided insights into the trend of the data. The flow range was from 25 μl/min to 160 ml/min and they used constant heater power as the heat source instead of constant temperature.[41]

In an improvement over the previous studies, our work features an application-oriented design and a 3D model where experiments and analytical results were verified. A sweat rate focused thermal flow rate sensor has yet to be investigated. In this study, we present a calorimetric sensor design for sweat rate detection based on theoretical calculations, finite element analysis simulations using COMSOL Multiphysics, and verification of the simulations with experimental data. With a number of sweat-based sensors being developed, sweat rate sensing offers a unique advantage of understanding the data from physiology perspective.

II. MATERIALS AND METHODS

The flow rate testing platform was built using a polydimethylsiloxane silicone elastomer kit (PDMS, Dow Corning). A 10:1 mixture of PDMS and curing agent was stirred for 5 min and placed in a vacuum degasser to remove air bubbles in the solution. The mixture was then poured into a mold for creating the sweat collector and channel and cured in an oven (Humboldt 30GC) at 70 °C for 2–3 h. The mold was prepared by using cut glass pieces that were glued on Silicon wafers. Channel dimensions were 26 mm × 3 mm × 1 mm. Inlets and outlets were created using a 1.2 mm puncher. 18 and 20 gauge tubings were used for inlets and outlets, respectively. A 10 Ω resistor (with 1 mm lead wiring) was used as the heating element. The ceramic coating of the resistor was removed to increase the heat transfer efficiency. Copper-Constantan T-type thermocouples (Omega) with 30 gauge (0.25 mm) wiring were used as the heating sensors. The standard limit of error was reported as 1 °C or 0.75% of the measurement value.[40] A Harrick plasma cleaner PDC-32 G (RF frequency of 8–12 MHz, input power of 100 W) was used to attach the patterned PDMS onto a glass slide substrate. Vinyl flexible adhesive (Loctite) was used around the base of the thermocouples and the heater on top of the PDMS surface.

Deionized water (resistivity 18.3 MΩ cm) was pumped through the channel with a syringe pump (KDS Scientific 100) to apply flow rates from 0.06 μl/min to 6 μl/min, which was considered to cover the range of human sweat rates.[34] 3 ml and 10 ml BD syringes were used for slow and fast flow rates, respectively. Air circulation and heat dissipation were limited by covering the setup loosely. The resistor was first heated to the desired temperature (47 °C) and the syringe pump was turned on once the temperature readings from the upstream and downstream thermocouple readings were stable. A power transistor (NPN MJE 200GOS) was used to provide the necessary current (approximately 80 mA) to the heating element. 5 V and 2.5V were applied to the collector and base of the transistor, respectively, using a BK Precision 1651A power supply. Temperature values were measured with a digital multimeter (Mastech MS 8268) and manually recorded every 15 s. MATLAB was used for further data processing.

Three dimensional numerical simulations were carried out using COMSOL Multiphysics. Dimensions for the simulation geometry were chosen to match the actual device. Laminar flow and heat transfer in fluids and solids were incorporated in the simulations. The heating element, i.e., the resistor, was represented by a Nichrome cylinder, while

Copper was chosen for the wires of the heating. Water was used as the fluid, since its thermal properties are very close to those of sweat. A layer of air was built around the device and its outer boundary temperature was set to 0 heat flux.

The volumetric flow rate (Q) can be given as:

$$Q = w\,h\,v, \tag{1}$$

where $w = 3$ mm and $h = 1.05$ mm are the width and length of the channel, respectively, and v is the flow velocity. The volumetric flow rate used in the experiments was between 0.3 μl/min (5×10^{-12} m^3/s) and 2.1 ml/min (3.5×10^{-8} m^3/s). However, simulations were carried out up to 1 l/min (1.667×10^{-5} m^3/s). Therefore, flow velocity for the device simulations was calculated between 5.29 μm/s and 5.29 m/s using Eq. (1). In the COMSOL model, the resistor heating element was set as the heat source with a fixed power density in W/m^3. Since a $R = 10\ \Omega$ resistor (a cylindrical shape of height $h_R = 5.3$ mm and radius $r_R = 0.8$ mm) was used for the experiments, a similar structure was designed in the 3D model. With a heater current of $I = 78$ mA, the heater power per volume was calculated as $P/V = I^2 \times R/(\pi r_R^2\, h_R) = 5.7$ MW/m^3.

In order to keep the simulations relevant with the real device, 10% of the resistor's cylindrical part was embedded in the channel. The rest of the resistor and its wires were also included in the 3D model. This cylindrical part was used as the heat source of the device, which depends on the power provided to the heater resistor and the volume of the heater. The device was designed to be wearable; hence, it will be in contact with the body. Therefore, the temperature of the bottom part of the device was chosen as 298.5 K (~25.4 °C), which is considered a typical skin temperature.

Finite element analysis applies the governing equations on each mesh. The accuracy of the solution increases with the number of increasing mesh elements, which results in longer simulation execution times. However, if the mesh is applied uniformly throughout the entire geometry, COMSOL automatically chooses the smallest mesh to solve the sharp corners in the geometry. However, this approach causes unnecessarily dense meshing in the large volumes (such as air or the substrate material). We used the Adaptive Mesh Refinement technique where the mesh size was determined depending on the complexity of the geometry areas. Tetrahedral meshing was utilized for the entire geometry and air blocks were coarsely meshed. Simulations were carried out in steady state and dynamic changes were not taken into account. The thermal conductivities of the materials are given in Table I.

A thermal imaging camera was used to find out the temperature profile of the heater and how it changes with the flow rate. The resolution of the FLIR A20 Infrared Imaging System was 0.6 mm with a minimum focus distance of 0.6 m. Similar to flow experiments, the flow was introduced by the syringe pump and temperature snapshots were taken for different flow rates. The camera was focused on the heater of the device.

III. PRINCIPLES OF CALORIMETRIC FLOW RATE SENSORS

A calorimetric flow meter consists of one heating element and two temperature sensors, namely, upstream and downstream sensors with respect to the heater. The temperature of the symmetrical upstream and downstream sensors with reference to the heater would be the same if there is no fluid flow. The length between the upstream sensor and the heater is defined as l_u and the length between the downstream sensor and the heater is represented with l_d as shown in Figure 1(a). When the fluid flow is increased, the upstream sensor temperature (T_u) starts to decrease due to the cooling effect of the fluid flow, eventually reaching room temperature as illustrated in Figure 1(b). However, the downstream sensor temperature (T_d) starts to increase since the heater temperature gradient is pushed towards downstream. This increase reaches a maximum when the cooling effect of the fluid flow overcomes the heater power and the heating element starts to cool down (Figure 1(b)). Therefore, T_d gradually decreases to reach to room temperature with very high flow rates. The temperature difference (ΔT) between two sensors is given as $T_u - T_d$. Figure 1(b) illustrates the temperature difference profile. It must be noted here that the flow rate value where T_d peaks depends on the power of the heating element, distance of the sensors from the heater, and material properties of the fluid and device.

The characteristic length (m^{-1}) of the heater (γ) can be expressed as[41]

$$\gamma_{1,2} = \frac{v \pm \sqrt{v^2 + \dfrac{16 a_{Fl}{}^2 k}{\delta^2}}}{4 a_{Fl} k}, \tag{2}$$

where v is the average flow velocity of the fluid (in m/s), a_{Fl} is the thermal diffusivity of the fluid (in m^2/s), δ is the thermal boundary layer thickness (in m), and k is a dimensionless factor and can be taken as 0.5.[41] For liquids with a small Reynolds number, δ can be considered as the height of the channel. The temperature difference between the two sensors (ΔT) is given as[41,43]

$$\Delta T = T_0\left[e^{\gamma_2 l_u} - e^{-\gamma_1 l_d}\right], \tag{3}$$

where T_0 is the heater temperature with respect to the room temperature and

$$T_0 = \frac{P}{\lambda_{Fl} b_H \left[\dfrac{l_H}{\delta} + \sqrt{\dfrac{v^2\delta^2}{4a_{fl}{}^2 + 4k}}\right]}, \tag{4}$$

TABLE I. Thermal conductivity values that were chosen for the materials used in the COMSOL model.

Material	Thermal conductivity [W/mK]
PDMS	0.16
Heating resistor	11.3
Thermocouples	400
Air	0.027 ± 0.001[a]

[a]COMSOL Multiphysics takes into account the fact that thermal conductivity of air is dependent on temperature. However, within the range of simulations (298 K–320 K), thermal conductivity only changes by 0.001 W/mK around the average value of 0.027 W/mK.

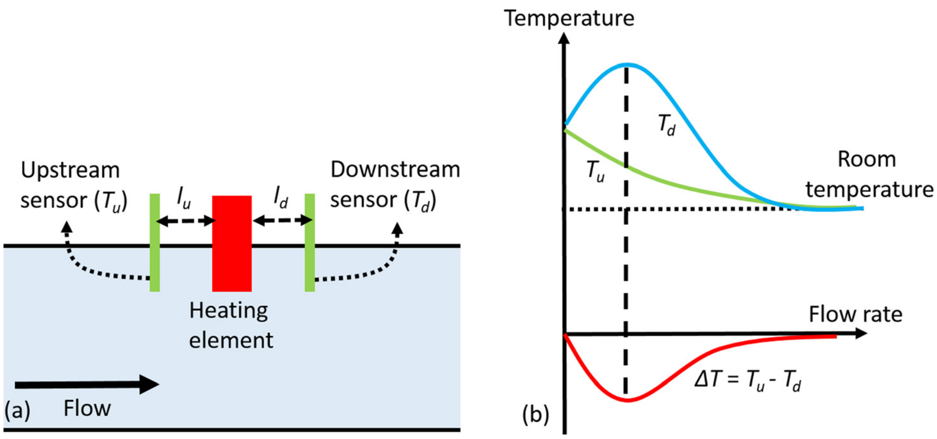

FIG. 1. Theoretical design and sensor readings for a calorimetric flow rate sensor; (a) cut view of the device with temperature sensors and the heating element and (b) theoretical temperature values for the upstream and downstream sensors. The maximum of the downstream sensor would be dependent on the flow velocity, which is a function of the flow rate and the device dimensions.

where P is the power (in W), λ_{Fl} is the thermal conductivity of water (in W/m K), b_H is the width of the heater (in m), and l_H is the length of the heater (in m). It can be seen from the heater temperature in (4) that the higher flow rates would cause the heater to cool down. This effect cannot be seen if a constant temperature was used as the heating source instead of constant power.

IV. RESULTS

The flow rate sensor was built using PDMS layers as shown in Figure 2. Resistor and thermocouples attached to the device were used to determine the flow rate. A Computer Aided Design (CAD) drawing similar to the one that was used for finite element analysis simulations is provided in Figure 2(a) for convenience. Inlet and outlet ports are also shown in Figure 2(b) where tubings were inserted. The thickness of the PDMS layers can be adjusted during the molding process by simply pouring less PDMS solution into the mold. Alternatively, the bottom PDMS layer that acts as a substrate could be replaced with any substrate material such as glass or any other flexible substrate.

As the heater power density is set to 5.7 MW/m^3, the main heating is caused by the heater rather than the outside temperature. Temperature profiles of three flow rates are plotted in Figure 3. At a slow flow rate (1 μl/min), temperature is uniformly distributed and the heater temperature reaches up to 323 K as shown in Figure 3(a). A medium flow rate (230 μl/min, Figure 3(b)) was chosen at a point where the temperature difference between sensing points is the maximum, i.e., temperature around the downstream sensor reaches its highest (hottest) value (320 K). The heater starts to cool down due to the flow (down to 318 K from 320). As the flow rate increases, water cools down the heater and thus the temperature difference starts to decrease and eventually reaches zero (1 l/min in Figure 3(c)) where both sensing locations are about the same temperature, close to room temperature. The heater is cooled down to 304 K, which is only 6 K higher than the room temperature.

It can be seen from Equation (4) that the temperature of the heater would decrease as the flow rate increases. It would eventually cool to room temperature, i.e., the temperature of the incoming liquid. This phenomenon is plotted in Figure 4 where both 3D simulations and analytical model results were provided. It must be noted here that the 3D simulations do take into account three dimensional effects whereas the analytical model does not consider such effects.

Figure 5 shows the temperature difference between the upstream and downstream sensor locations. Experiments were only conducted up to 2.1 ml/min due to limitations of the setup. However, an actual sweat rate would be up to a few μl/min, which is much lower than this limit. The reason that the simulations were run for a wider range was to show the theoretical minimum in ΔT where the dissipated power by the flow starts to cool down the heater significantly such that the downstream sensor does not warm up any further. Temperature values of the experiments and the simulation results agree well, which shows that the model could be used for further analysis. Furthermore, Equation (4) was also used to plot the temperature difference, which has a similar trend to the experiments and 3D simulations. It is important to note here that the analytical model calculations do not include 3D effects.

While the current device and its related simulation results serve as an important proof of concept, they are not

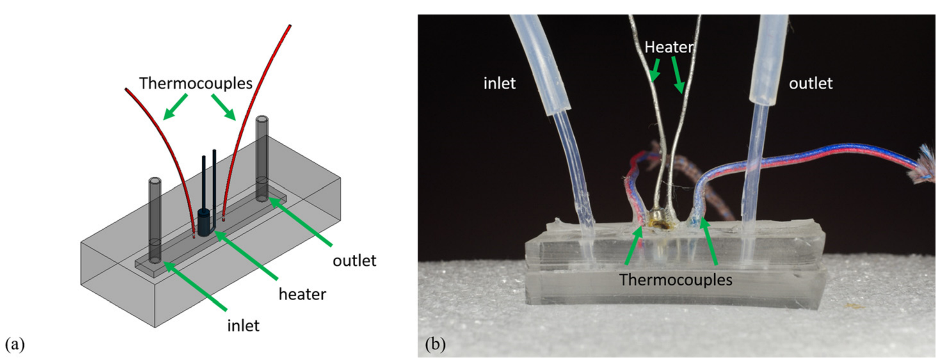

FIG. 2. Actual flow rate sensor device that was used in the experiments; (a) isometric view of the device and (b) the actual photo of the device.

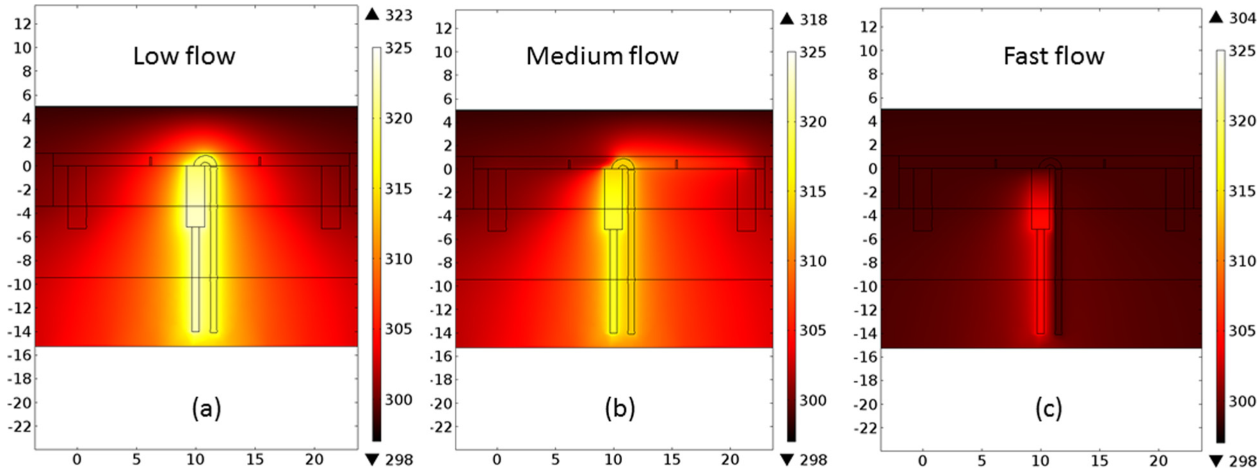

FIG. 3. Temperature distribution for different flow rates; (a) slowest (1 μl/min), (b) medium (230 μl/min), and (c) fast (1 l/min) flow rate. Higher flow rates cause the heating element to cool down.

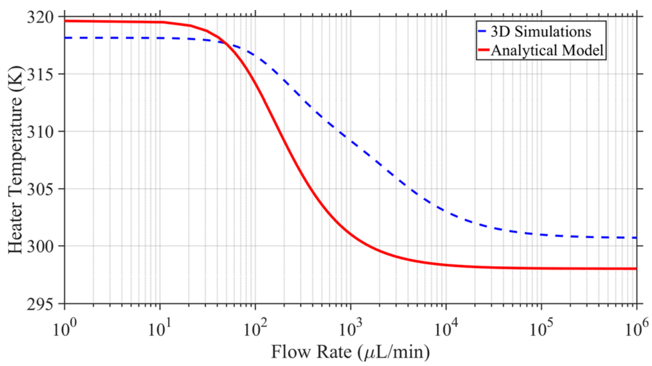

FIG. 4. Heater temperature decreases with an increasing flow rate and ultimately reaches to room temperature. 3D simulations and analytical model results show a similar trend.

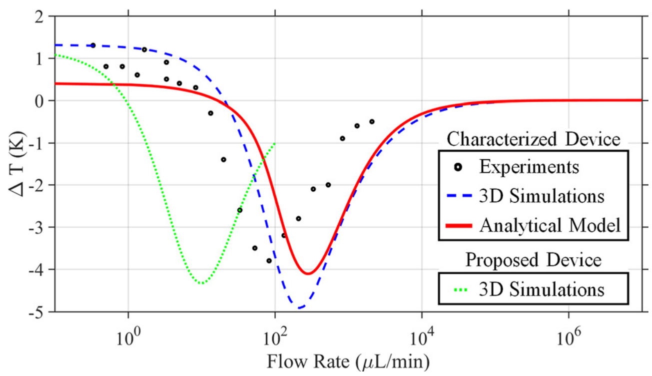

FIG. 5. Temperature difference (ΔT) between the upstream and downstream sensors. The experimental data follow a similar trend to the 3D simulations and analytical model results using Equations (2)–(4).[41] A proposed, scaled down version of the device was simulated to provide a realistic flow rate range for human sweat.

yet suitable for a real sweat sensor device because the human sweat rates range from 0.5 μl/min to 10 μl/min. It is seen from Figure 5 that ΔT does not change significantly within the human sweat rate range. In order to show the viability of the design, another set of simulations was run, where the device dimensions were scaled down 20 times from the current design, and the heater power was adjusted accordingly. This resulted in a shift of the minimum to lower flow rate values. The simulation result of the proposed, scaled device is also shown in Figure 5. Detailed dimensions of the proposed device will be provided in the Discussion section.

In order to better understand the temperature profiles, a thermal imaging camera was used. It can be seen in Figure 6(a) that the temperature around the part of the resistor exposed to air reaches up to 330 K for slow flows (1 μl/min in Figure 6(a)), which is 10 K warmer than what we observed in the simulations (Figure 3). However, temperature dissipates quite rapidly with the distance and ranges around 300 K inside the device. As the flow is increased (100 μl/min in Figure 6(b)), the heater temperature decreases slightly (down to 328 K from 330 K) and the temperature distribution in the channel shifts towards downstream.

V. DISCUSSION

A simple estimate of the heat flow can be done as follows: For a given volume flow rate Q, the sweat mass flow rate is $m = \rho Q$, where ρ is the density of the water (1 g/cm^3). Assuming that the water gets heated by $\Delta T = 10\,^\circ$C as it passes the heater, the dissipated power becomes

$$P = c\rho Q\,\Delta T, \tag{5}$$

where c is the specific heat of water (4.186 Joule/g °C). The current that passes through the 10 Ω resistor is about 78 mA. Therefore, the power that is delivered to the resistor is calculated as 60 mW. The ceramic insulation layer of the resistor was removed to improve the thermal contact between the fluid and the heater. Because only a fraction of the resistor is inside the flow channel (the rest is embedded in the PDMS), it can be assumed that the maximum heating power in the channel would be less than 60 mW. The dissipated power from the heat source would be equal to 60 mW at around 67 μl/min. At this flow rate, it is expected that the heater will start to cool down. This phenomenon was observed at 230 μl/min where the heating source was set at 240 mW. This result means that only 25% of the heating was transferred into the flow channel.

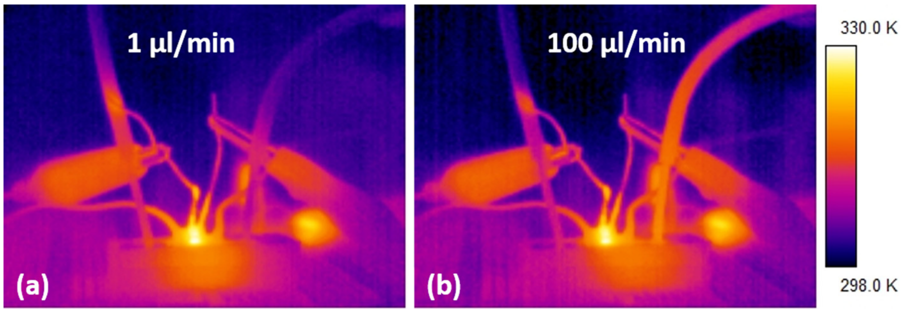

FIG. 6. Thermal camera image of the resistor for (a) 1 μl/min and (b) 100 μl/min flow rates.

It can be seen from Figure 5 that the minimum temperature difference for the experiments and the simulations occurs at a different flow rate. This difference is mainly due to the inaccurate calculation of the channel dimensions. Although the channel dimensions were measured, due to debris from the insertion of tubes, sensors, and resistors, the channel is perhaps narrower than the original measurements. Smaller channel dimensions would increase the flow velocity in the channel, hence shifting the minimum. The temperature difference should reach zero with high flow rates due to heating element cooling, which is clearly seen from both simulations and experiments. The temperature difference at a slow flow rate is due to the asymmetry of the device and locations of the temperature sensor (i.e., how far the sensor is inserted into the channel).

In an application as a sweat flow sensor, the device would measure the temperature difference $\Delta T = T_u - T_d$, which would then be converted to a flow rate via a calibration curve. For best sensitivity, a small change in the flow rate should correspond to a large temperature change ΔT. According to Figure 5, this condition is best fulfilled at flow rates between 10 and 100 μl/min. Since actual sweat rates are typically no more than a few μl/min, the sensitivity of the device could be improved by further narrowing the channel, thus increasing the flow velocity. In order to show the applicability and viability of this proposal, we have carried out simulations (shown in Figure 5) where we scaled down the device dimensions 20 times. The new channel width, depth, and length became 50 μm, 150 μm, and 1.25 mm, respectively. These dimensions could easily be implemented by traditional soft lithography techniques. Furthermore, the sizes of the heater and temperature sensors are of the order of micrometers, which can also be manufactured using standard microfabrication techniques (i.e., metal deposition and patterning). The heater power density was also increased to 1865 MW/m^3 from 5.7 MW/m^3 in order to keep the temperature difference in the same range. This increase was a result of the scaling down of the height and radius of the cylindrical heater (h_R and r_R, respectively) in accordance with the heater power density ($I^2 \times R/(\pi r_R{}^2\, h_R)$). With the new device dimensions, the region of best flow rate discrimination (i.e., the largest negative slope in Fig. 5) is shifted down to values between 1 and 10 μl/min, i.e., typical human sweat rates.

VI. CONCLUSION

In this paper, we developed a calorimetric flow rate sensor using discrete components such as thermocouples as temperature sensors and a resistor as the heating element. This simple yet efficient device design approach allowed us to understand the fundamentals of microflow rate sensing, which can be adapted into sweat rate sensor research which is quite crucial for exercise physiologists. We have developed a 3D model using COMSOL Multiphysics, which gave us a unique advantage of furthering the knowledge of temperature effects for a flow rate sensor. We covered a wide range of flow rates with our experiments including the average sweat rate values for humans. Simulations extended the flow rate coverage to show the cooling effects even further. Furthermore, a verified 3D model was used to propose a scaled down version of the device that could directly be used for human sweat rate applications.

This proof-of-concept device assumes that sweat is properly collected and fed into the channel. There are several ways to introduce the sweat into the channel. The authors previously proved that a PDMS based or a 3D printed sweat collector can be used to gather the sweat and analyze sweat conductivity real-time.[20,44] Other sweat collection methods were also proposed that can be incorporated with the current design. Flexible hydrophilic materials such as wicked textile and paper microfluidic patches were used as sweat collectors.[45,46]

Endurance sports are constantly seeking new ways to improve the performance of individual athletes. Several studies focused on sweat compound sensing but there has yet to be significant advances in measuring the sweat rate, which is relatively slow, i.e., on the order of μl/min. We not only proposed a new approach to sweat rate sensing but also developed a solid 3D model that can be used to test different environmental conditions without doing actual tests.

ACKNOWLEDGMENTS

Susanne Marie Wroblewski from the Center for Merchandising and Design Technology of Central Michigan University helped with the thermal images. Dr. Juan Peralta helped with the actual device photo. Jun Lu and Nitish Vaja assisted with the CAD drawing. Dr. Jinxiang Xi helped us with the initial COMSOL model. Chris Gargarello worked on the initial prototype of the device. Andrew Brueck helped us with a final proofreading.

[1]D. J. Casa, L. E. Armstrong, S. J. Montain, B. S. E. Rich, and J. A. Stone, J. Athl. Train. **35**, 212 (2000).
[2]L. E. Armstrong, D. L. Costill, and W. J. Fink, Med. Sci. Sports Exercise **17**, 456 (1985).
[3]R. M. Walsh, T. D. Noales, and J. A. Hawley, Int. J. Sports Med. **15**, 392 (1994).

[4]B. Murray, J. Am. Coll. Nutr. **26**, 542S (2007).
[5]M. N. Sawka, Med. Sci. Sports Exercise **24**, 657 (1992).
[6]N. A. Taylor and C. A. Machado-Moreira, Extreme Physiol. Med. **2**, 1 (2013).
[7]K. Sato, W. H. Kang, K. Saga, and K. T. Sato, J. Am. Acad. Dermatol. **20**, 537 (1989).
[8]F. T. Amorim, A. C. Vimieiro-Gomes, C. A. Machado-Moreira, F. C. Magalhães, M. S. Rosa, L. S. Prado, and L. O. C. Rodrigues, J. Therm. Biol. **31**, 521 (2006).
[9]S. F. Godek, C. Peduzzi, R. Burkholder, S. Condon, G. Dorshimer, and A. R. Bartolozzi, J. Athl. Train. **45**, 364 (2010).
[10]L. B. Baker, J. R. Stofan, A. A. Hamilton, and C. A. Horswill, J. Appl. Physiol. **107**, 887 (2009).
[11]N. B. Morris, M. N. Cramer, S. G. Hodder, G. Havenith, and O. Jay, J. Appl. Physiol. **114**, 816 (2013).
[12]D. Gagnon and G. P. Kenny, J. Appl. Physiol. **113**, 746 (2012).
[13]M. J. Buono, K. D. Ball, and F. W. Kolkhorst, J. Appl. Physiol. **103**, 990 (2007).
[14]K. Sato, W. H. Kang, K. Saga, and K. T. Sato, J. Am. Acad. Dermatol. **20**, 713 (1989).
[15]G. W. Cage and R. L. Dobson, J. Clin. Invest. **44**, 1270 (1965).
[16]I. L. Schwartz and J. H. Thaysen, J. Clin. Invest. **35**, 114 (1956).
[17]H. Tanaka, Y. Osaka, S. Obara, H. Yamaguchi, and H. Miyamoto, Eur. J. Appl. Physiol. Occup. Physiol. **64**, 557 (1992).
[18]M. J. Buono, R. Claros, T. DeBoet, and J. Wong, J. Appl. Physiol. **105**, 1044 (2008).
[19]J. R. Allan and C. G. Wilson, J. Appl. Physiol. **30**, 708 (1971).
[20]G. Liu, C. Ho, N. Slappey, Z. Zhou, S. E. Snelgrove, M. Brown, A. Grabinski, X. Guo, Y. Chen, K. Miller, J. Edwards, and T. Kaya, Sens. Actuators, B **227**, 35 (2016).
[21]S. M. Shirreffs and R. J. Maughan, J. Appl. Physiol. **82**, 336 (1997).
[22]H. Ueda and Y. Inoue, J. Ergono. **3**, 1000121 (2013).
[23]G. Havenith, A. Fogarty, R. Bartlett, C. J. Smith, and V. Ventenat, Eur. J. Appl. Physiol. **104**, 245 (2008).
[24]M. J. Patterson, S. D. R. Galloway, and M. A. Nimmo, Exp. Physiol. **85**, 869 (2000).
[25]J. R. Stofan, J. J. Zachwieja, C. A. Horswill, R. Murray, S. A. Anderson, and E. R. Eichner, Int. J. Sport. Nutr. Exerc. Metab. **15**, 641 (2005).
[26]L. B. Baker, C. T. Ungaro, K. A. Barnes, R. P. Nuccio, A. J. Reimal, and J. R. Stofan, Physiol. Rep. **2**, 1 (2014).
[27]R. W. Bullard, J. Appl. Physiol. **17**, 735 (1962).
[28]A. C. Machado-Moreira, F. M. Smith, A. M. Van den Heuvel, I. B. Mekjavic, and N. A. Taylor, Eur. J. Appl. Physiol. **104**, 265 (2008).
[29]Y.-J. Fan, Trop. Med. **29**, 107 (1987).
[30]M. R. Ely, B. R. Elly, T. D. Chinevere, C. P. Lacher, H. C. Lukaski, and S. N. Cheuvront, Physiol. Meas. **33**, 385 (2012).
[31]P. Wei, B. Morey, T. Dyson, N. McMahon, Y. Y. Hsu, S. Gazman, L. Klinker, B. Ives, K. Dowling, and C. Rafferty in *The IEEE Sensors 2013: Proceedings of the IEEE Sensors, Baltimore, Maryland, USA, 4–6 November 2013* (2013), pp. 1–4.
[32]P. Salvo, F. D. Francesco, D. Costanzo, C. Ferrari, M. G. Trivella, and D. D. Rossi, IEEE. Sens. J. **10**, 1557 (2010).
[33]S. Coyle, K. T. Lau, N. Moyna, D. O'Gorman, D. Diamond, F. D. Francesco, D. Costanzo, P. Salvo, M. G. Trivella, D. E. D. Rossi, N. Taccini, R. Paradiso, J.-A. Porchet, A. Ridolf, J. Luprano, C. Chuzel, T. Lanier, F. Revol-Cavalier, S. Schoumacker, V. Mourier, I. Chartier, R. Convert, H. De-Moncuit, and C. Bini, IEEE Trans. Inf. Technol. Biomed. **14**, 364 (2010).
[34]G. Matzeu, C. Fay, A. Vaillant, S. Coyle, and D. Diamond, IEEE Trans. Biomed. Eng. **63**, 1672 (2015).
[35]J. T. Kuo, L. Yu, and E. Meng, Micromachines **3**, 550 (2012).
[36]M. Elwenspoek, in *Thermal Flow Micro Sensors 1999: Proceedings of the Semiconductor Conference, 1999, Sinaia, Romania, 5–9 October 1999* (1999), pp. 423–435.
[37]A. Arevalo, E. Byas, and I. G. Foulds, in *Proceedings of 2013 COMSOL Conference, Rotterdam, Holland* (2013).
[38]A. Rasmussen, C. Mavriplis, M. E. Zaghloul, O. Mikulchenko, and K. Mayaram, Sens. Actuators, A. **88**, 121 (2001).
[39]C. Ho, A. T. Iftekhar, and T. Kaya, in Simulation and Characterization of a Micro-Scale Calorimetric Flow Rate Sensor for Sweat Rate Detection 2016: Proceedings of the IEEE Engineering in Medicine and Biology Society, Orlando, Florida, USA, 16–20 August 2016 (2016).
[40]See http://www.omega.com/prodinfo/thermocouples.html for thermocouples (last accessed on September 26, 2016).
[41]N. T. Nguyen and W. Dötzel, Sens. Actuators, A. **62**, 506 (1997).
[42]N. Sabate, J. Santander, L. Fonseca, I. Gracia, and C. Cane, Sens. Actuators, A. **110**, 282 (2004).
[43]T. S. J. Lammerink, N. R. Tas, M. Elwenspoek, and J. H. J. Fluitman, Sens. Actuators, A. **37**, 45 (1993).
[44]G. Liu, M. Alomari, B. Sahin, S. E. Snelgrove, J. Edwards, A. Mellinger, and T. Kaya, Appl. Phys. Lett. **106**, 133702 (2015).
[45]B. Schazmann, D. Morris, C. Slater, S. Beirne, C. Fay, R. Reuveny, N. Moyna, and D. Diamond, Anal. Methods **2**, 342 (2010).
[46]D. P. Rose, M. Ratterman, D. K. Griffin, L. Hou, N. Kelley-Loughnane, R. R. Naik, J. A. Hagen, I. Papautsky, and J. Heikenfeld, IEEE Trans. Biomed. Eng. **62**, 1457 (2015).